DOI 10.1515/htmp-2012-0132 — High Temp. Mater. Proc. 2013; 32(3): 247–254

In-Ho Jung*, Pierre Hudon, Wan-Yi Kim, Marie-Aline van Ende, Miftaur Rahman and Gabriel Garcia Curiel

Thermodynamic Database of P_2O_5-containing Oxide Systems for the Dephosphorization Process in Steelmaking

Abstract: The Na_2O-MgO-CaO-FeO-Fe_2O_3-Al_2O_3-SiO_2-P_2O_5 system is a basic oxide system for the Basic Oxygen Furnace (BOF) process as well as the hot metal dephosphorization process. Numerous experimental investigations on this oxide system are being carried out to find out an advanced process route for P removal from molten iron. In spite of their industrial importance, however, phase equilibria in oxide systems containing P_2O_5 have not been well investigated due to the complexity of their chemistry. No systematic thermodynamic modeling of these systems has been conducted to date, either. In order to meet the strong demands of steelmaking and other industries, new systematic thermodynamic modeling of the P_2O_5-containing oxide systems (Na_2O-MgO-CaO-FeO-Fe_2O_3-Al_2O_3-SiO_2-P_2O_5) and key phase diagram experiments have been carried out over the past years. In the present study, the results of the thermodynamic modeling of unary, binary and ternary P_2O_5-containing systems and the applications of the thermodynamic database to the dephosphorization by multi-component slag in BOF process are presented in comparison with experimental data. All thermodynamic calculations were performed using FactSage thermodynamic software.

Keywords: dephosphorization, BOF process, thermodynamic database

***Corresponding author: In-Ho Jung:** Department of Mining and Materials Engineering, McGill University, Montreal, Quebec, Canada
E-mail: in-ho.jung@mcgill.ca
Pierre Hudon, Wan-Yi Kim, Marie-Aline van Ende, Miftaur Rahman, Gabriel Garcia Curiel: Department of Mining and Materials Engineering, McGill University, Montreal, Quebec, Canada

1 Introduction

The CaO-FeO-Fe_2O_3-MgO-SiO_2-Al_2O_3-P_2O_5 system is a basic oxide system for the Basic Oxygen Furnace (BOF) process as well as the hot metal dephosphorization process. Numerous investigations on this oxide system are being carried out to find out an advanced process route for P removal from molten iron. In the modern steelmaking process, the BOF process is a key step for dephosphorization and decarburization. Unfortunately, a deep understanding of the process is still out of reach in many aspects due to the complex slag chemistry involved and the difficulty in sampling/examination during the process. In particular, a large amount of industrial efforts were spent to improve the efficiency of P removal from the hot-metal with minimum Fe loss during the BOF process. Two advanced BOF process technologies recently used by several advanced steel producers are:

- The double slag BOF process technology, where most of the molten slag is discharged after the dephosphorization process at low temperature and the decarburization is conducted afterwards with a new synthetic slag.
- The double BOF furnaces technology, where one furnace is dedicated to the dephosphorization process at low temperature and the other one to the decarburization process at high temperature.

In order to understand the BOF process and improve it further in particular for the dephosphorization reaction, a good thermodynamic understanding of phosphorus behavior in a wide range of slag compositions (from Fe_tO-SiO_2 rich slag to CaO-SiO_2-Fe_tO-MgO slag), temperatures (between 1200 and 1750°C) and oxygen potentials (from very oxidizing conditions to carbon saturation condition) is indispensable. In addition, a good comprehension of the influence of other components such as Al_2O_3, MnO, Na_2O, etc. on the phosphorus distribution between molten iron and multicomponent slags is essential. The phosphorus distribution between molten slag and solid Ca_2SiO_4, which can dissolve a considerable amount of P_2O_5 under steelmaking conditions, is also an important issue in the temperature range of 1200 to 1600°C. Although many experimental studies have been conducted to measure the phosphorus distribution between multicomponent slags and molten iron and determine the phosphate

capacity of slags, a more accurate knowledge on P_2O_5-containing slags is needed to improve the dephosphorization process. This is especially true if one wants to develop a simulation model for the BOF process, where a computerized thermodynamic database for P_2O_5 containing slags is highly required.

Over the past 30 years, advances in thermodynamic modeling have resulted in the development of computer databases containing thermodynamic properties as functions of temperature and composition of hundreds of multicomponent oxide phases. One of the most well known and widely used oxide databases is the FACT oxide database [1]. The FACT oxide database contains the complete description of the CaO-Al_2O_3-SiO_2-MgO-FeO-Fe_2O_3 system with additional components like MnO_x, CrO_x, TiO_x, *etc*. However, in the case of P_2O_5, the current FACT oxide database is quite restricted within dilute compositions and the accuracy of the calculations is less satisfactory.

In order to meet the strong demands of the steelmaking and other industries, new systematic thermodynamic modeling of P_2O_5-containing systems (CaO-FeO-Fe_2O_3-SiO_2-MgO-Al_2O_3-Na_2O-P_2O_5) and key phase diagram experiments have been carried out over the past years. In the present study, the results of the thermodynamic modeling of unary, binary and ternary P_2O_5-containing systems and the applications of the thermodynamic database to the dephosphorization by multi-component slags in the BOF process are presented in comparison with experimental data. All thermodynamic calculations were performed using FactSage thermodynamic software.

2 Thermodynamic modeling

A thermodynamic database for the multicomponent system CaO-FeO-Fe_2O_3-MgO-SiO_2-Al_2O_3-Na_2O-P_2O_5 has been developed in our research group based on a critical evaluation and optimization of all available phase diagram and thermodynamic data for unary, binary and ternary systems. In this way, the Gibbs energy of all phases in the given system can be expressed as functions of temperature, composition and pressure, and their model parameters can be stored in a computerized data-file. In the present study, the thermodynamic behavior of the liquid phase was described using the Modified Quasichemical Model [2], which considers the short-range-ordering of second nearest neighbor cations. The details of the model description can be found elsewhere [2].

The thermodynamic properties of pure P_2O_5 are not well-known as well. Consequently, a critical thermodynamic evaluation of pure P_2O_5 was properly carried out for the first time using all available equilibration data for gaseous, solid and liquid P_2O_5 [3]. Interestingly, the well-accepted Gibbs energy of formation (ΔG_f^o) of liquid P_2O_5 from Turkdogan and Pearson in 1953 [4] is not consistent with the experimental phase diagram data of P_2O_5:

$$P_2(g) + 5/2\ O_2(g) = P_2O_5(l) \quad (1)$$

– Turkdogan and Pearson [4]

$$\Delta G_f^o = -1534482 + 506.3\ T\ (\text{J/mol});\quad \log K = -16.35 \text{ at } 1873\ K \quad (2)$$

– Present study [3]

$$\Delta G_f^o = -1616372 + 539.0\ T\ (\text{J/mol});\quad \log K = -16.92 \text{ at } 1873\ K \quad (3)$$

In the present study, the new ΔG_f^o of P_2O_5(l) is evaluated based on all available thermodynamic data of the P_2O_5 system. The evaluated Gibbs energy of formation is given in Eq. (3) and the calculated phase diagram of the present study is depicted in Figure 1. If the previous value by Turkdogan and Pearson [4] is used, the melting temperature of P_2O_5 becomes less than 300°C, while experimental data give 580°C. Surprisingly, the difference in log K for reaction (1) between the present study and the previous data of Turkdogan and Pearson [4] is just about 0.5~0.6 in the temperature range of 1300 to 1700°C.

It should be noted that solid P_2O_5 has three polymorphs: hexagonal (H-P_2O_5) and two orthorhombic (O-P_2O_5 and O'-P_2O_5). According to the experimental data

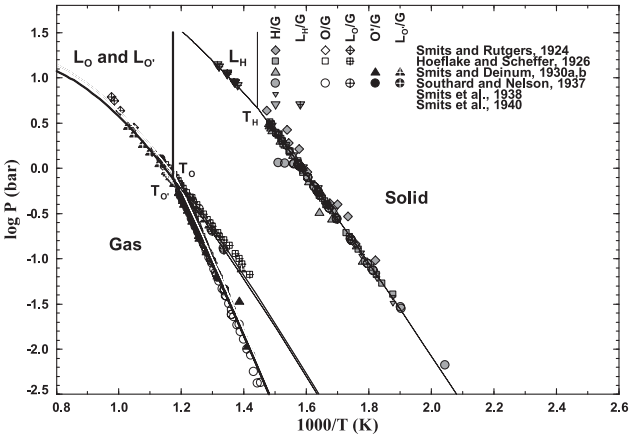

Fig. 1: Log P vs 1000/T diagram of the P_2O_5 unary used in the present study. O'-P_2O_5 is the most stable solid phase and melts at 580°C. Details of the thermodynamic modeling results can be found in reference [2].

Table 1: Optimized model parameters of the Modified Quasichemical Model for the CaO-P_2O_5 slag (J mol^{-1}).

$Z^{Ca}_{CaCa} = 1.37744375$; $Z^{P2O3}_{P2O3P2O3} = 4.1322000$
$\Delta g_{Ca\text{-}P2O3} = (-435914.224 + 41.300264\,T) - 37530.48\,X_{Ca\text{-}Ca}$
$- 123900.792\,X_{P2O3\text{-}P2O3}$
$+ (-186955.19916 + 41.835816\,T)\,X^2_{P2O3\text{-}P2O3}$
$+ 76427.09876\,X^4_{P2O3\text{-}P2O3}$

and T-P diagram of P_2O_5 in Figure 1, O-P_2O_5 transforms into O'-P_2O_5 at about 70°C and O'-P_2O_5 melts at 580°C. That is, H-P_2O_5 is metastable in all temperature ranges at 1 atm. Both, the JANAF thermodynamic table [5] and the SGTE pure substance database [6], have no thermodynamic data for the most stable solid phase O'-P_2O_5. One should be therefore careful to take the thermodynamic data of P_2O_5 from these sources. A discussion on the thermodynamic properties of P_2O_5 can be found elsewhere [3].

Binary MO-P_2O_5 (M = Ca, Mg, Fe, Mn), SiO_2-P_2O_5, Al_2O_3-P_2O_5, Fe_2O_3-P_2O_5 and Na_2O-P_2O_5 systems were optimized based on all available experimental thermodynamic and phase diagram data. In the case of the binary CaO-P_2O_5 system, for example, many intermediate compounds $xCaO{\cdot}yP_2O_5$ and a liquid phase exist. Among the solid phases, the thermodynamic properties, including enthalpy of formation at 298 K, entropy at 298 K, both low and high temperature heat capacities, enthalpy of fusion, and Gibbs energy of formation of $Ca_4P_2O_9$, $Ca_3P_2O_8$, $Ca_2P_2O_7$ and CaP_2O_6 are relatively well investigated by experiments. The model parameters of the liquid solution in the CaO-P_2O_5 system are listed in Table 1. The details of the thermodynamic modeling results will be published elsewhere [7]. During the thermodynamic optimization, all available original thermodynamic data and phase diagram data [8–28] were critically evaluated and simultaneously optimized to obtain one set of Gibbs energy functions for each phase in the system, as shown in Figures 2 and 3.

The optimized MgO-P_2O_5 phase diagram and its calculated P_2O_5(l) and MgO(l) activities are presented in Figures 4 and 5, respectively, with experimental data [20, 29–44]. In a similar way, all the available experimental data concerning the phase diagram and thermodynamic properties of all other binary MgO-, FeO-, Fe_2O_3-, MnO-, Al_2O_3-, Na_2O- and SiO_2-P_2O_5 systems were critically evaluated and optimized to obtain the binary interactions between the oxide component and P_2O_5 in liquid slag.

The most fundamental system for the dephosphorization of slag in the BOF process is the CaO-Fe_tO-P_2O_5 system. Many experimental studies have been performed to determine the phase diagram and phosphorus distribution between the slag and molten iron in the temperature

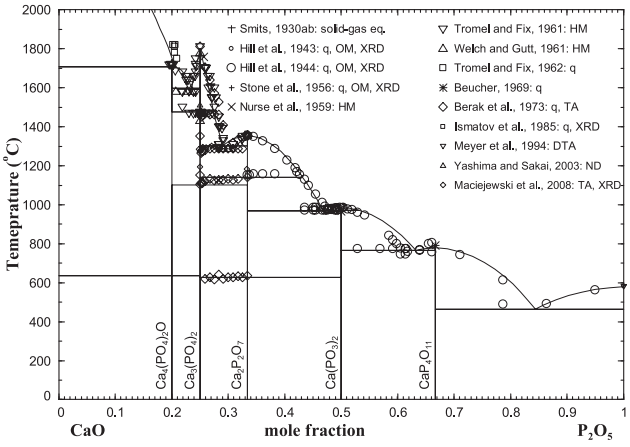

Fig. 2: Optimized binary phase diagram of the CaO-P_2O_5 system with experimental data [8–22].

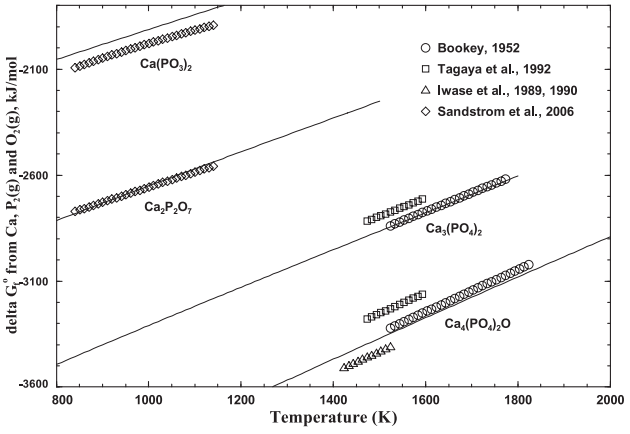

Fig. 3: Optimized Gibbs energy of formation of intermediate compounds in the CaO-P_2O_5 system in comparison with experimental data [23–28].

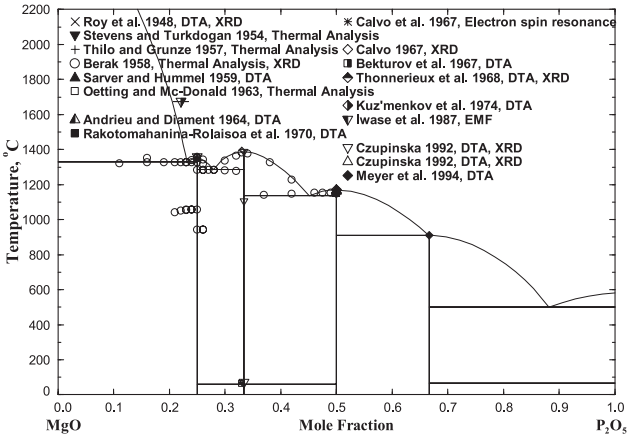

Fig. 4: Optimized binary phase diagram of the MgO-P_2O_5 system with experimental data [20, 29–44].

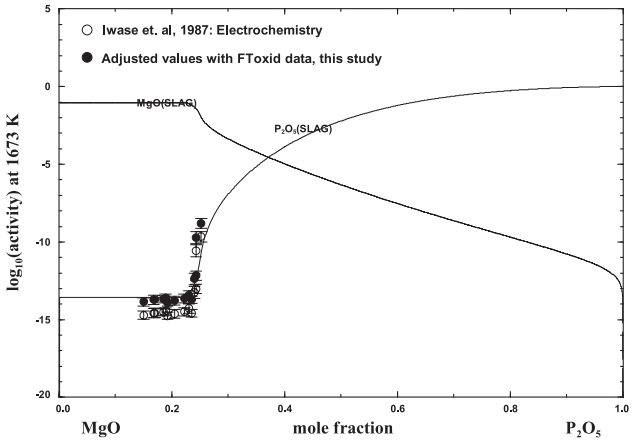

Fig. 5: Calculated activity of P_2O_5(l) in the MgO-P_2O_5 system along with experimental data [42]. The Gibbs energy of pure liquid P_2O_5 of Iwase et al. [42] was corrected according to the new P_2O_5 Gibbs energy by Jung and Hudon [3] to ensure a thermodynamically consistent database development.

range of 1550 and 1750°C. As it can be seen in Figure 6 (a), the phase diagram of the CaO-Fe_tO-P_2O_5 system at 1600°C is well reproduced by the thermodynamic modeling. It should be noted that the liquid miscibility gap along the $Ca_3P_2O_8$ and FeO diagonal is reasonably reproduced as well. Many researchers have investigated the phosphorus distribution ($L_P = (\%P)_{slag}/[\%P]_{Fe}$) and the relationship between [%P] in molten iron along with the Fe_tO concentration in molten slag saturated with CaO or $4CaO{\cdot}P_2O_5$. The calculated L_P and [%P] at various temperatures are compared with experimental data [16, 45–51] in Figure 6 (b) and (c), respectively. The L_P data in Figure 6 (b) are well reproduced in a wide range of compositions and temperatures, and the changes in the location of maximum L_P are also well reproduced within the experimental error limits. In the case of [%P] in molten iron (Figure 6 (c)), the P content drops drastically with increasing FeO content in slag, which is very well reproduced by the present thermodynamic calculations.

3 Application to dephosphorization in the BOF process

The most important thermodynamic parameter to determine the dephosphorization capacity of the slag is the activity coefficient of P_2O_5 in the liquid slag. The activity coefficient can be determined by the interaction of P_2O_5 and other slag components. Of course, the binary interaction parameters are most influential to the activity coefficient. In the present study, optimized binary liquid model

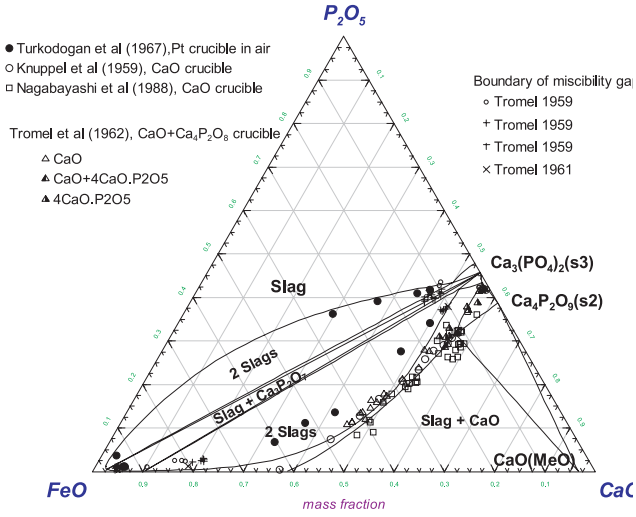

(a)

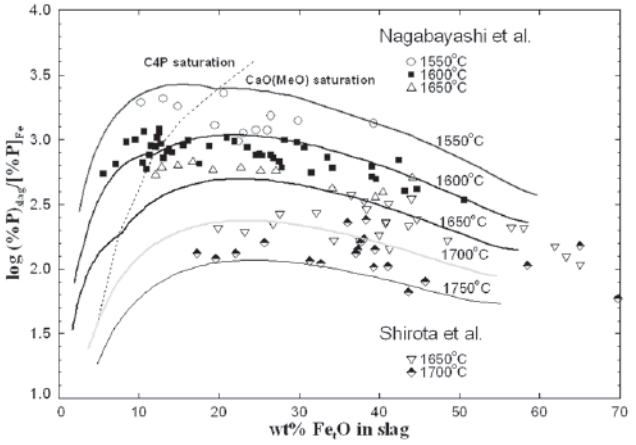

(b)

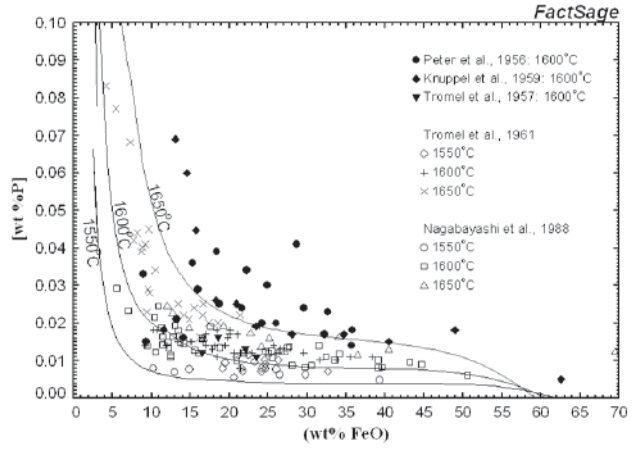

(c)

Fig. 6: (a) The calculated phase diagram of the CaO-Fe_tO-P_2O_5 system equilibrated with molten Fe at 1600°C, (b) L_P between molten iron and the slag along CaO saturation line, and (c) the relationship between [%P] in liquid Fe and Fe_tO content in slag along CaO saturation line in comparison with available experimental data [16, 45–51].

parameters (interaction parameters between P_2O_5 and other oxide components in liquid slag), which can reproduce all thermodynamic properties and phase diagram in the binary systems, were used to predict the dephosphorization of multi-component slags. That is, in the present study, the interaction parameters were not determined to simply reproduce the dephosphorization behavior of multicomponent slag.

The BOF slag is typically based on the CaO-Fe_tO-SiO_2 system. MgO is also intentionally added to protect the refractory lining of the BOF furnace (MgO-C), while small amounts of Al_2O_3, MnO, TiO_2, Na_2O and CaF_2 are added or naturally formed from the reactions with molten pig iron during the process. As it is well-known, the main purpose of the BOF process is the decarburization and dephosphorization of steel. Although C can be exhausted as CO or CO_2 gas by reacting with injected oxygen, the phosphorus in molten Fe ends up as P_2O_5 in the molten slag where it can reach several wt.%.

The calculated phase diagram of the CaO-Fe_tO-SiO_2 slag with 10 and 15 wt.% MgO saturated with molten Fe at 1600°C, which is projected onto the CaO-Fe_tO-SiO_2 ternary, is shown in Figure 7. In the calculation, 0.5 wt.% P_2O_5 was added to calculate the L_P values between slag and molten metal. Suito et al. [52] and Selin [53] investigated the phosphorus distribution in this system using MgO crucibles. The MgO saturation line (liquidus of $MgO_{s.s.}$) from these two experimental studies is rather different especially in the FeO-rich corner. The calculated MgO saturation line from the present database is consistent with Selin [53] rather than Suito et al. [52]. The calculated L_P values from the present thermodynamic database are in good agreement with the experimental results near the Ca_2SiO_4 saturation region. When the FeO concentration is increased in both, Figure 7 (a) and (b), our L_P values are in good agreement with those of Selin [53]. Because the L_P values are highly dependent on the amount of CaO and FeO, the L_P data from Suito et al. [52] and Selin [53] show more difference in the FeO-rich corner. The L_P data of Suito et al. [52] are in general slightly higher than the values of Selin [53] because the slags in Suito et al.'s study [52] are more CaO-enriched at the same FeO concentration.

A large amount of experimental data for the dephosphorization distributions between multicomponent slags (CaO-MgO-SiO_2-Fe_tO-Na_2O-Al_2O_3-MnO-P_2O_5 system) and liquid iron at temperatures from 1100 to 1700°C were collected from literature [16, 45, 47, 51–70] and reviewed in the present study. Thermodynamic calculations between the slag and molten iron were performed using the present thermodynamic database based on each experimental condition. Experimental data [16, 45, 47, 51–70] and calculated values are compared in Figure 8. The L_P data for binary, ternary, quaternary and multicomponent systems from the literature were collected and the calculations performed using the same experimental conditions. More than 1000 experimental points [16, 45, 47, 51–70] are compared in Figure 8.

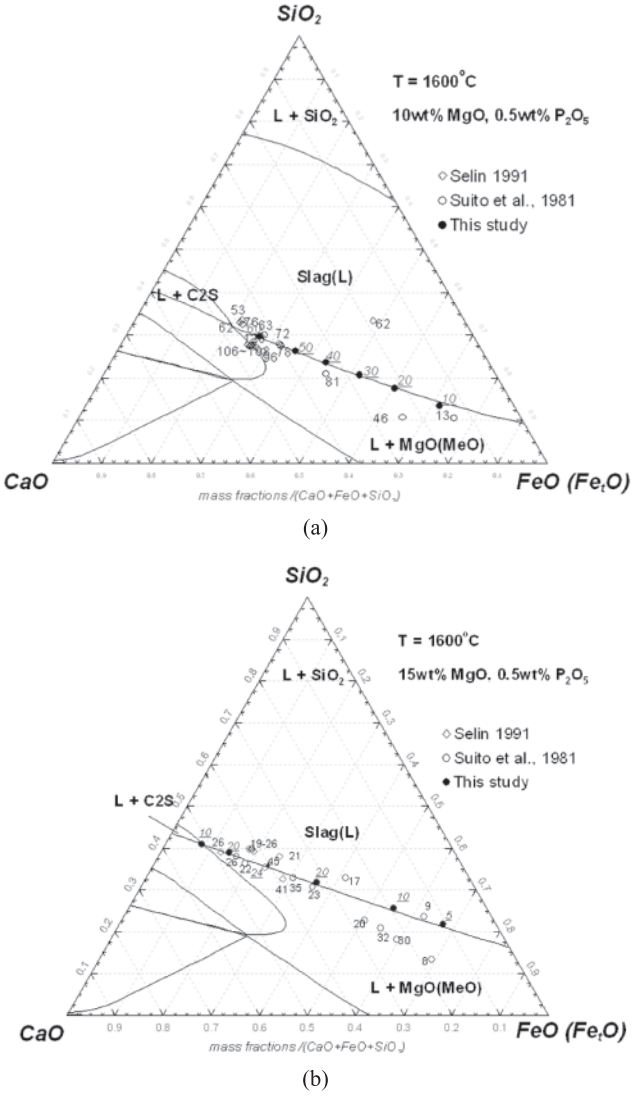

Fig. 7: Calculated phosphorus distribution between slag and molten Fe for the CaO-Fe_tO-SiO_2-MgO slag at 1600°C in comparison with experimental data [52–53]. (a) CaO-Fe_tO-SiO_2-10% MgO slag and (b) CaO-Fe_tO-SiO_2-15% MgO slag. Upright numbers in the diagram are experimental L_P data and underlined numbers are the calculated L_P values from the present database.

To examine in more details the slag system relevant to the BOF process, the experimental data for the phosphorus distribution between the CaO-MgO_{sat}-SiO_2-Fe_tO-(MnO) slag and molten iron are compared with calculations in Figure 9. The L_P data were determined at temperatures between 1550 and 1700°C by many researchers under Ar

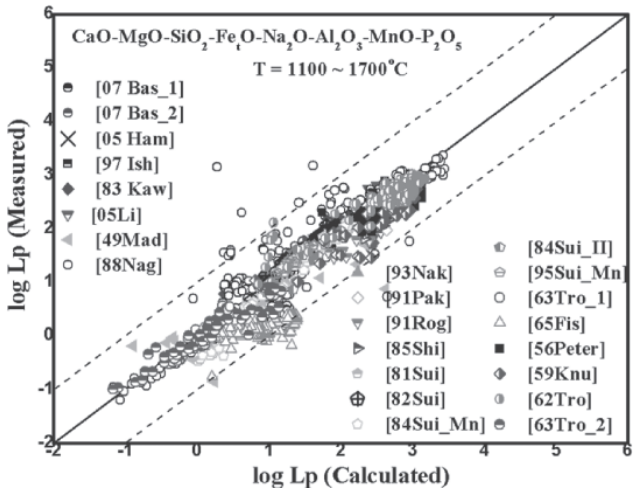

Fig. 8: Comparison between experimental [16, 45, 47, 51–70] and calculated L_P values for binary, ternary and multicomponent slags using the present thermodynamic database.

gas with MgO crucibles [51–53, 60–61, 69–70]. The comparison between the measured L_P data and calculated L_P values shows an excellent agreement with each other.

It is very well known that phosphorus can be dissolved in solid Ca_2SiO_4 phase. According to the phase diagram, Ca_2SiO_4 and $Ca_3P_2O_8$ form a complete solid solution. In the BOF process, this dissolution of P_2O_5 in Ca_2SiO_4 is important for dephosphorization control. The solid solution was modeled in the present study considering the CaO-SiO_2-P_2O_5 phase diagram and in particular the Ca_2SiO_4-$Ca_3P_2O_8$ pseudo-binary section. The phosphorous distribution between Ca_2SiO_4 solid solution and the CaO-FeO-Fe_2O_3-SiO_2 system has been investigated recently under air and reduced oxygen partial pressure. The calculated L_P ($L_P = (\%P_2O_5)_{Ca2SiO4\ solution}/(\%P_2O_5)_{slag}$) from the present thermodynamic database and recent experimental data are in good agreement. The L_P data are typically much higher than 1, which means when CaO-FeO-Fe_2O_3-SiO_2 slags are saturated with Ca_2SiO_4 solid phase, a large portion of P_2O_5 can be dissolved into Ca_2SiO_4, which can be an effective way to increase dephosphorization of liquid iron.

The present thermodynamic database has been already applied to the BOF process simulation [71]. The equilibrium reaction zone volume model was used to simulate the kinetics of chemical reaction at each reaction zone in the BOF process. In preliminary simulations, the variations of chemical composition, temperature and amount of liquid metal and slag are predicted with processing time. Currently, a more sophisticated and versatile BOF process model is under development in collaboration with several steelmakers to use the present thermodynamic database more actively for the process control system.

4 Summary

In order to meet the strong demands of the steelmaking industry, new systematic thermodynamic modeling of the P_2O_5-containing systems (CaO-FeO-Fe_2O_3-SiO_2-MgO-Al_2O_3-Na_2O-P_2O_5) and new key phase diagram experiments have been carried out. Phase diagrams and thermodynamic properties data available for unary, binary and ternary P_2O_5-containing systems were critically evaluated and optimized to build up a reliable thermodynamic database. In order to describe the thermodynamic behavior of P_2O_5 in slag, the Modified Quasichemical Model taking into

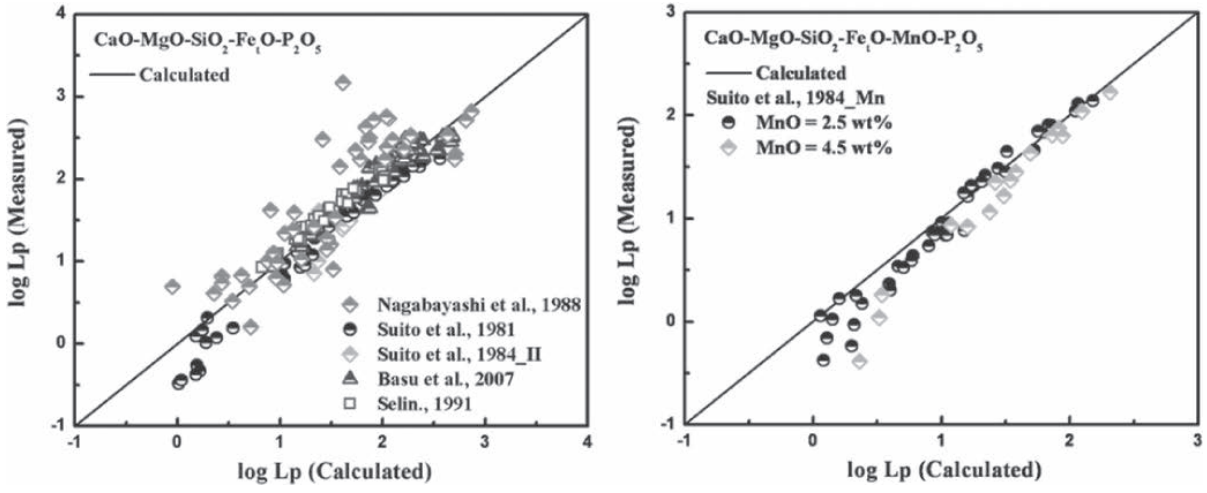

Fig. 9: Comparison between experimental and calculated L_P values for the CaO-MgO-SiO_2-Fe_tO(-MnO) system [51–53, 60–61, 69–70].

account the short-range-ordering of cations in molten slag is used explicitly in the present study. The optimized model parameters for binary and ternary P_2O_5 systems can be used to predict the phosphorus distribution between multicomponent slags and molten iron over a wide range of temperature and oxygen partial pressure. The calculated L_P values from the present thermodynamic database are in good agreement with experimental L_P data within experimental error limits. We believe that the present thermodynamic database can be used to simulate the complex BOF process, which can be helpful to understand the chemical reactions taking place during the BOF process and eventually become an important tool for the development of an environmentally more sustainable BOF process in the future.

Acknowledgement: Financial support from Tata Steel Europe, Posco, RIST, Hyundai Steel, Nucor steel, RTIT, Nippon Steel Corp., JFE steel, Sumitomo metals, Voestalpine Stahl, RHI, and the Natural Sciences and Engineering Research Council of Canada are gratefully acknowledged.

Received: August 8, 2012. Accepted: December 14, 2012.

References

[1] C. W. Bale, E. Bélisle, P. Chartrand, S. A. Decterov, G. Eriksson, K. Hack, I. H. Jung, Y. B. Kang, J. Melançon, A. D. Pelton, C. Robelin and S. Petersen, *Calphad*, **33** (2009), pp. 295–311.
[2] A. D. Pelton, S. A. Degterov, G. Eriksson, C. Robelin and Y. Dessureault, *Metall. Mater. Trans. B*, **31B** (2000), pp. 651–659.
[3] I.-H. Jung and P. Hudon, *J. Am. Ceram. Soc.*, **95** (2012), pp. 3665–3672.
[4] E. T. Turkdogan and J. Pearson, *J. Iron Steel Inst., London*, **175** (1953), pp. 398–401.
[5] M. W. Chase Jr, NIST-JANAF Thermochemical Tables, Fourth Edition, Part II, Cr-Zn, p. 1810 In *Journal of Physical and Chemical Reference Data Monograph No. 9*, The American Chemical Society and The American Institute of Physics, Woodbury, NY (1998).
[6] A. T. Dinsdale, *Calphad*, **15** (1991), pp. 317–425.
[7] P. Hudon and I. H. Jung, unpublished work.
[8] A. Smits and H. W. Deinum, *Proc. K. Ned. Akad. Wet.*, **33** (1930), pp. 514–525.
[9] I. A. Smits, *Z. physik. Chem.*, **149** (1930), pp. 337–363.
[10] W. L. Hill, G. T. Faust and S. B. Hendricks, *J. Am. Chem. Soc.*, **65** (1943), pp. 794–802.
[11] W. L. Hill, G. T. Faust and D. S. Reynolds, *Am. J. Sci.*, **242** (1944), pp. 457–477,542–462.
[12] P. E. Stone, E. P. Egan, Jr. and J. R. Lehr, *J. Am. Ceram. Soc.*, **39** (1956), pp. 89–98.
[13] R. W. Nurse, J. H. Welch and W. Gutt, *J. Chem. Soc.*, (1959), pp. 1077–1083.
[14] G. Tromel and W. Fix, *Arch. Eisenhuttenwes.*, **32** (1961), pp. 209–212.
[15] J. H. Welch and W. Gutt, *J. Chem. Soc.*, (1961), pp. 4442–4444.
[16] G. Tromel and W. Fix, *Arch. Eisenhuttenwes.*, **33** (1962), pp. 745–755.
[17] M. Beucher, *Mater. Res. Bull.*, **4** (1969), pp. 15–18.
[18] J. Berak and T. Znamierowska, *Rocz. Chem.*, **47** (1973), pp. 1137–1149.
[19] A. A. Ismatov, S. Y. Azimov and R. I. Akhmedov, *Uzb. Khim. Zh.*, (1985), pp. 66–68.
[20] K. Meyer, H. Hobert, A. Barz and D. Stachel, *Vib. Spectrosc.*, **6** (1994), pp. 323–332.
[21] M. Yashima, A. Sakai, T. Kamiyama and A. Hoshikawa, *J. Solid State Chem.*, **175** (2003), pp. 272–277.
[22] M. Maciejewski, T. J. Brunner, S. F. Loher, W. J. Stark and A. Baiker, *Thermochim. Acta*, **468** (2008), pp. 75–80.
[23] J. B. Bookey, *J. Iron Steel Inst., London*, **172** (1952), pp. 61–66.
[24] A. Tagaya, F. Tsukihashi, N. Sano, Y. Nabika and T. Hashimoto, *Iron Steelmaker*, **18** (1991), pp. 63–69.
[25] A. Tagaya, F. Tsukihashi, N. Sano, Y. Nabika and T. Hashimoto, *Trans. Iron Steel Soc.*, **13** (1992), pp. 59–65.
[26] M. Iwase, H. Fujiwara, E. Ichise, H. Kitaguchi and K. Ashida, *Iron Steelmaker*, **16** (1989), pp. 45–52.
[27] M. Iwase, H. Fujiwara, E. Ichise, H. Kitaguchi and K. Ashida, *Trans. Iron Steel Soc.*, **11** (1990), pp. 31–38.
[28] M. H. Sandstroem, D. Bostroem and E. Rosen, *J. Chem. Thermodyn.*, **38** (2006), pp. 1371–1376.
[29] R. Roy, E. T. Middleswarth and F. A. Hummel, *Am. Mineral.*, **33** (1948), pp. 458–471.
[30] C. G. Stevens and E. T. Turkdogan, *Trans. Faraday Soc.*, **50** (1954), pp. 370–373.
[31] E. Thilo and I. Grunze, *Z. Anorg. Allg. Chem.*, **290** (1957), pp. 209–222.
[32] J. Berak, *Rocz. Chem.*, **32** (1958), pp. 17–22.
[33] J. F. Sarver and F. A. Hummel, *J. Electrochem. Soc.*, **106** (1959), pp. 500–504.
[34] F. L. Oetting and R. A. Mc-Donald, *J. Phys. Chem.*, **67** (1963), pp. 2737–2743.
[35] R. Andrieu and R. Diament, *Compt. Rend.*, **259** (1964), pp. 4708–4711.
[36] C. Calvo, J. S. Leung and W. R. Datars, *J. Chem. Phys.*, **46** (1967), pp. 796–803.
[37] C. Calvo, *Acta Crystallogr.*, **23** (1967), pp. 289–295.
[38] A. B. Bekturov, D. Z. Serazetdinov, Y. A. Kushnikov, E. V. Poletaev and S. M. Divnenko, *Zh. Neorg. Khim.*, **12** (1967), pp. 2355–2362.
[39] B. Thonnerieux, J. C. Grenier, A. Durif and C. Martin, *C. R. Acad. Sci., Paris, Ser. C*, **267** (1968), pp. 968–970.
[40] M. I. Kuz'menkov, S. V. Plyshevskii and V. V. Pechkovskii, *Izv. Akad. Nauk SSSR, Neorg. Mater.*, **10** (1974), pp. 1842–1845.
[41] E. Rakotomahanina-Rolaisoa, Y. Henry, A. Durif and C. Raholison, *Bull. Soc. Fr. Mineral. Cristallogr.*, **93** (1970), pp. 43–51.
[42] M. Iwase, H. Akizuki, H. Fujiwara, E. Ichise and N. Yamada, *Steel Res.*, **58** (1987), pp. 215–219.
[43] G. Czupinska, *J. Therm. Anal.*, **38** (1992), pp. 2343–2347.
[44] G. Czupinska, *Thermochim. Acta*, **202** (1992), pp. 77–78.
[45] O. Peter, d. E. W. vor and W. Oelsen, *Arch. Eisenhuttenwes.*, **27** (1956), pp. 219–230.

[46] G. Tromel and H. W. Fritze, *Arch. Eisenhuttenwes.*, **28** (1957), pp. 489–495.
[47] H. Knuppel, F. Oeters and H. Gruss, *Arch. Eisenhuttenwes.*, **30** (1959), pp. 253–265.
[48] G. Tromel and H. W. Fritze, *Arch. Eisenhuttenwes.*, **30** (1959), pp. 461–472.
[49] G. Tromel, W. Fix and H. W. Fritze, *Arch. Eisenhuttenwes.*, **32** (1961), pp. 353–359.
[50] K. Schwerdtfeger and E. T. Turkdogan, *Trans. Metall. Soc. AIME*, **239** (1967), pp. 589–590.
[51] R. Nagabayashi, M. Hino and S. Banya, *Tetsu to Hagane*, **74** (1988), pp. 1770–1777.
[52] H. Suito, R. Inoue and M. Takada, *Trans. Iron Steel Inst. Jpn.*, **21** (1981), pp. 250–259.
[53] R. Selin, *Scand. J. Metall.*, **20** (1991), pp. 279–299.
[54] W. R. Maddocks and E. T. Turkdogan, *J. Iron Steel Inst., London*, **162** (1949), pp. 249–264.
[55] G. Tromel and K. Schwerdtfeger, *Arch. Eisenhuttenwes.*, **34** (1963), pp. 101–108.
[56] G. Tromel and K. Schwerdtfeger, *Arch. Eisenhuttenwes.*, **34** (1963), pp. 55–59.
[57] W. A. Fischer and H. J. Fleischer, *Arch. Eisenhuttenwes.*, **36** (1965), pp. 791–798.
[58] H. Suito and R. Inoue, *Trans. Iron Steel Inst. Jpn.*, **22** (1982), pp. 869–877.
[59] Y. Kawai, H. Nakamura, K. Kawakami, T. Toyoda, A. Ishizaka and T. Ebisawa, *Tetsu to Hagane*, **69** (1983), pp. 1755–1762.
[60] H. Suito and R. Inoue, *Trans. Iron Steel Inst. Jpn.*, **24** (1984), pp. 257–265.
[61] H. Suito and R. Inoue, *Trans. Iron Steel Inst. Jpn.*, **24** (1984), pp. 40–46.
[62] Y. Shirota, K. Katohgi, K. Klein, H. J. Engell and D. Janke, *Trans. Iron Steel Inst. Jpn.*, **25** (1985), pp. 1132–1140.
[63] J. J. Pak and R. J. Fruehan, *Metall. Trans. B*, **22B** (1991), pp. 39–46.
[64] S. Nakamura, F. Tsukihashi and N. Sano, *ISIJ Int.*, **33** (1993), pp. 53–58.
[65] H. Suito and R. Inoue, *ISIJ Int.*, **35** (1995), pp. 266–271.
[66] H. Ishii and R. J. Fruehan, *Iron Steelmaker*, **24** (1997), pp. 47–54.
[67] T. Hamano and F. Tsukihashi, *ISIJ Int.*, **45** (2005), pp. 159–165.
[68] G. Li, T. Hamano and F. Tsukihashi, *ISIJ Int.*, **45** (2005), pp. 12–18.
[69] S. Basu, A. K. Lahiri and S. Seetharaman, *Metall. Mater. Trans. B*, **38B** (2007), pp. 623–630.
[70] S. Basu, A. K. Lahiri and S. Seetharaman, *Metall. Mater. Trans. B*, **38B** (2007), pp. 357–366.
[71] I. H. Jung, M. A. Van Ende and W. Y. Kim, *CAMP-ISIJ*, **25** (2012), pp. 199–202.